NR4A1 mediates chemotherapy-induced senescence via the PI3K/AKT pathway in gastric cancer cells

TINGYU ZHANG[1,2], YUE WANG[1,2], JIUNA ZHANG[3], XUESHUAI YE[4], YANFENG SHEN[2] and ZHIWEI ZHANG[1,2]

[1]School of Clinical Medicine, Hebei University of Engineering, Handan, Hebei 056000, P.R. China;
[2]Department of Oncology, The Affiliated Hospital of Hebei University of Engineering, Handan, Hebei 056000, P.R. China;
[3]Department of Gastroenterology, The Affiliated Hospital of Hebei University of Engineering, Handan, Hebei 056000, P.R. China;
[4]Central Laboratory, The Affiliated Hospital of Hebei University of Engineering, Handan, Hebei 056000, P.R. China

Received November 13, 2025; Accepted January 19, 2026

DOI: 10.3892/or.2026.9080

Abstract. Gastric cancer (GC) remains among the cancers with extremely high morbidity and mortality rates worldwide, and chemotherapy resistance limits its therapeutic efficacy. Therapy-induced senescence (TIS) is vital for inducing chemotherapy resistance and promoting tumor progression, highlighting the need to explore its regulatory mechanisms. To investigate oxaliplatin (OXA)-induced senescence in GC cells, cellular senescence was assessed by senescence-associated β-galactosidase (SA-β-Gal) staining, western blotting, immunofluorescence, and reverse transcription-quantitative polymerase chain reaction for the senescence-associated secretory phenotype (SASP) factors. Moreover, multi-omics integration including transcriptomic, proteomic and untargeted metabolomic, was used to identify key regulators and pathways. OXA induced a senescent phenotype characterized by p21 upregulation, SA-β-Gal staining, cell cycle arrest and SASP secretion. Integrative multi-omics analysis revealed that NR4A1 is a central upstream regulator, and the PI3K/AKT pathway is suppressed in OXA-induced senescence. Notably, survival analysis verified that NR4A1 expression was correlated with the prognosis of patients in GC. Functional studies demonstrated that NR4A1 knockdown attenuated OXA-induced senescence, restored PI3K/AKT activity, and reduced SASP expression. Metabolomic profiling revealed that OXA-induced senescence induced metabolic reprogramming, including glycolysis enhancement and oxidative phosphorylation suppression. Notably, NR4A1 knockdown reversed these metabolic alterations. The present study identified NR4A1 as a key regulated gene in chemotherapy-induced senescence in GC and verified that the NR4A1/AKT-metabolism axis is vital for the pivotal mechanism of TIS. These findings may provide a novel therapeutic strategy to optimize chemotherapy and develop 'one-two punch' approaches targeting senescent tumor cells.

Correspondence to: Dr Zhiwei Zhang or Mr. Yanfeng Shen, Department of Oncology, The Affiliated Hospital of Hebei University of Engineering, 81 Congtai Road, Congtai, Handan, Hebei 056000, P.R. China
E-mail: zhangzw128@126.com
E-mail: 15690009299@163.com

Key words: gastric cancer, cellular senescence, NR4A1, PI3K/AKT pathway, multi-omics, metabolic reprogramming

Introduction

Gastric cancer (GC) remains a gastrointestinal cancer with high global incidence and mortality (1). Despite major advances in perioperative chemotherapy and immunotherapy, the overall survival (OS) of patients with advanced disease remains poor. The widespread development of chemoresistance poses a major clinical challenge. Previous studies have revealed that radiotherapy and platinum-based and other chemotherapy drugs can trigger therapy-induced senescence (TIS) by inducing DNA damage or replication stress (2,3). As an inherent cellular stress response, TIS has a dual role in cancer treatment. Senescent cells enter stable cell cycle arrest, suppressing tumor proliferation. Conversely, residual senescent cells can secrete senescence-associated secretory phenotype (SASP) factors, remodel the tumor immune microenvironment, foster immune evasion, and potentially drive tumor recurrence (4). Consequently, a promising 'one-two punch' strategy has gained traction, which aims to trigger senescence and then specifically to clear or reprogram (5,6).

At the molecular level, the PI3K/AKT pathway is commonly dysregulated in GC, driving tumor cell proliferation and viability, regulating metabolic reprogramming, and contributing to resistance to cytotoxic drugs (7,8). Therefore, this is regarded as an important mechanism of treatment resistance and disease recurrence in GC. PI3K/AKT, as the 'master switch' of tumor metabolism, controls glucose and lipid metabolism, macromolecule biosynthesis and autophagy (9). Moreover, senescent cells exhibit unique vulnerability to PI3K/AKT inhibition (10,11), providing a potential opportunity for subsequent 'senolysis' interventions. Metabolic reprogramming, particularly the balance reconstruction of oxidative phosphorylation (OXPHOS) and glycolysis, regulates TIS (12,13).

Clinically, platinum-based regimens are vital for the first-line treatment of GC. Previous studies indicate that

platinum drugs can trigger cellular senescence in various tumor models, accompanied by cell cycle arrest and enhanced SASP secretion (14,15). The stress response nuclear receptor NR4A1 has emerged as a remarkable molecular bridge, linking these chemotherapeutic stimuli to the senescent phenotype. As a cellular stress sensor, NR4A1 coordinates critical signaling and metabolic adaptations and its ability to regulate pathways, including PI3K/AKT, makes it a credible mediator of chemotherapy-induced senescence. Consequently, simultaneously exploiting NR4A1-mediated PI3K inhibition to drive metabolic reprogramming during chemotherapy-induced senescence may amplify the antitumor effect of senescence and create opportunities for combining senolytic or immunotherapy strategies.

This investigation demonstrated that under chemotherapy-induced stress, the NR4A1-PI3K/AKT axis drives metabolic reprogramming and promotes the acquisition and maintenance of the senescence state in GC cells. Clarifying this molecular mechanism may provide actionable therapeutic targets for optimizing the 'one-two punch' sequential treatment strategy. This may offer novel approaches to overcome chemotherapy resistance and prevent GC recurrence.

Materials and methods

Cell culture and senescence induction. AGS and MKN45 human GC cell lines were acquired from the Procell Life Science & Technology Co., Ltd. and maintained in RPMI-1640 containing 10% FBS (Gibco; Thermo Fisher Scientific, Inc.) at 37˚C with 5% CO_2 condition. Senescence was induced by treating AGS cells with 2.5 μM oxaliplatin (OXA) and MKN45 cells with 5 μM OXA for 48 h.

Cell Counting Kit-8 (CCK-8) assay. To determine the 50% inhibitory concentration and GC cells were plated in 96-well plates ($3.0x10^3$ cells/well) and treated with a gradient of OXA concentrations: 0, 1.25, 2.5, 5, 10, 20, 40 and 80 μM. After 48 h, 10 μl CCK-8 reagent (Beyotime Institute of Biotechnology) was added per well, followed by a 1 h incubation in the dark at 37˚C. Absorbance at 450 nm was recorded with a microplate reader (EPOCH-SN; BioTek Instruments, Inc.).

Senescence-associated β-galactosidase (SA-β-Gal) staining. Cellular senescence was assessed with a commercial kit (Beyotime Institute of Biotechnology). Cells were rinsed with phosphate-buffered saline (PBS), fixed, incubated with SA-β-Gal staining solution overnight at 37˚C without CO_2, and then washed with PBS. Images were captured using an optical microscope (IX73; Olympus Corporation), and the percentage of SA-β-Gal-positive cells was quantified.

Western blotting. GC cells were lysed using RIPA buffer (Beijing Solarbio Science & Technology Co., Ltd.) with protease inhibitors (Beyotime Institute of Biotechnology). Protein concentration was then measured with a BCA kit (Beyotime Institute of Biotechnology). Proteins (20 μg per lane) were resolved by 10-15% SDS-PAGE and then transferred onto PVDF membranes (MilliporeSigma). Membranes were blocked with 5% non-fat milk at room temperature (RT) for 2 h, washed with TBST (0.1% Tween-20). They were then incubated with primary antibodies overnight at 4˚C and subsequently with secondary antibodies for 1 h at RT. Protein band was developed with ECL reagent (Beyotime Institute of Biotechnology), captured with an Amersham Image Quant 800 imaging system (Amersham; Cytiva), and analyzed for gray-level. Antibody details were listed in Table SI.

Immunofluorescence. Cells ($1.0x10^5$) were fixed with 4% paraformaldehyde, blocked with 3% BSA (Wuhan Servicebio Technology Co., Ltd.) for 30 min at RT. Cells were then incubated overnight at 4˚C with a primary antibody against phospho-H2A.X (1:100; cat. no. GB111841; Wuhan Servicebio Technology Co., Ltd.), followed by incubation with a Cy3-conjugated goat anti-rabbit IgG secondary antibody (1:300; cat. no. GB21303; Wuhan Servicebio Technology Co., Ltd.) for 50 min at RT. Nuclei were visualized by DAPI (2.0 μg/ml) counterstaining for 10 min. Images were captured using a Nikon Eclipse C1 fluorescence microscope (Nikon Corporation). Antibody details were listed in Table SI.

Reverse transcription-quantitative PCR (RT-qPCR). Total RNA was isolated and reverse transcribed into cDNA using commercial kits (Tiangen Biotech Co., Ltd.) according to the manufacturer's instructions. RT-qPCR was conducted with SYBR Green Master Mix (Tiangen Biotech Co., Ltd.) under the following thermocycling protocol: 95˚C for 2 min, 95˚C for 5 sec, 60˚C for 10 sec and 72˚C for 15 sec for 40 cycles. Relative gene expression was calculated using the $2^{-\Delta\Delta Cq}$ method (16). Primers were listed in Table SII.

Experimental design for multi-omics analysis. AGS cells were divided into two experimental groups: An untreated control group and an oxaliplatin-induced senescent group. For transcriptomic, proteomic and untargeted metabolomics analyses, four independent biological replicates were included for each group (n=4 per group).

Transcriptomic sequencing. Total RNA was isolated with TRIzol reagent (Beyotime Institute of Biotechnology). RNA concentration was measured using a NanoDrop 2000 spectrophotometer (Thermo Fisher Scientific, Inc.). RNA samples with a concentration ≥10 ng/μl and a total amount ≥1 μg were considered qualified for subsequent library construction. RNA integrity was verified by 1% RNase-free agarose gel electrophoresis stained with GelRed. cDNA libraries were constructed with the Hieff NGS® Ultima Dual mode mRNA Library Prep Kit (cat. no. 12309ES; Shanghai Yeasen Biotechnology Co., Ltd.) and were then amplified by PCR. Library concentration was evaluated using the DNA1000 assay Kit (cat. no. 5067-1504; Agilent Technologies, Inc.), and the final library loading concentration was 3 ng/μl. Sequencing was performed on an Illumina NovaSeq X Plus platform with a paired-end 150 bp strategy by Gene Denovo Biotechnology Co., Ltd.

Next, using DESeq2 software, differentially expressed genes (DEGs) were selected based on the criteria of |fold change| ≥2 and an adjusted $P<0.05$. Volcano plots and heatmaps were plotted with the online Omicsmart platform (http://www.omicsmart.com). Kyoto Encyclopedia of Genes and Genomes (KEGG) enrichment analysis was performed on DEGs.

Proteomic analysis. Following protein extraction and enzymatic digestion, the peptides were separated by an UltiMate 3000 liquid chromatography system (Thermo Fisher Scientific, Inc.) and analyzed using a timsTOF Pro2 mass spectrometer from Bruker Daltonics. DIA proteomics data were analyzed using Spectronaut 18 (Biognosys AG) under default parameters. The ideal extraction window was dynamically determined by the Spectronaut using iRT calibration and gradient stability. A false discovery rate threshold of 1% was applied at both the precursor and protein levels. Peptides passing this filter were quantified using the MaxLFQ algorithm to generate normalized protein group abundances. Mass spectrometric data were acquired in DIA mode using diaPASEF. Differentially expressed proteins were defined by a |fold change| >1.2 and a Benjamini-Hochberg adjusted P<0.05.

Untargeted metabolomics. The samples were mixed with methanol/acetonitrile/H_2O (2:2:1, v/v/v). Next, mixtures were sonicated twice on ice for 30 min each and centrifuged at 14,000 x g (20 min, 4˚C). The supernatant was collected and evaporated under vacuum. Dried extracts were redissolved in an acetonitrile aqueous solution, centrifuged, and the supernatant was collected for injection. Separation was conducted on an Agilent 1290 Infinity UHPLC system interfaced with an AB Sciex TripleTOF 6600 Q-TOF mass spectrometer, and quality control was conducted using QC samples. Data from the positive (pos) and negative (neg) ion modes were processed independently. Raw data were transformed into the mzML format utilizing ProteoWizard. Subsequent processing, including peak alignment, retention time correction, and extraction of peak area, was carried out with XCMS software.

Metabolite identification and data preprocessing were then performed; the steps were as follows: Features with missing values exceeding 50% were removed; remaining missing values were filled using k-nearest neighbor imputation; and features with a relative standard deviation greater than 50% were filtered out. Significantly altered metabolites were selected with the variable importance in projection (VIP) score ≥1 in OPLS-DA model, followed by filtering with a univariate t-test (P<0.05).

Gene expression profiling interactive analysis (GEPIA2) survival analysis. The prognostic significance of NR4A1 expression in GC was evaluated via the GEPIA2 platform (http://gepia2.cancer-pku.cn/), which combines RNA-seq data from The Cancer Genome Atlas (TCGA) and the Genotype-Tissue Expression projects (17). For the OS analysis, TCGA-stomach adenocarcinoma (STAD) cases were segregated into 'high' and 'low' NR4A1 expression groups according to the median transcripts per million values as the cut-off. Survival outcomes between groups were compared using Kaplan-Meier analysis with the log-rank (Mantel-Cox) test. The hazard ratio along with 95% confidence intervals was calculated.

Cell transfection. The short hairpin RNA (shRNA) NR4A1 lentiviral vector was constructed by Shanghai GeneChem Co., Ltd., using the pFU-GW backbone. The sequences for the shRNAs are as follows: A non-targeting control (sh-NC, 5'-TTCTCCGAACGTGTCACGT-3') and three NR4A1-specific sequences (sh-NR4A1#1 sense: 5'-TGGTGAAGGAAGTTGTCCGAA-3', antisense: 5'-TTCGGACAACTTCCTTCACCA-3'; sh-NR4A1#2 sense: 5'-GATTGACAGTATCCTGGCCTT-3', antisense: 5'-AAGGCCAGGATACTGTCAATC-3'; sh-NR4A1#3 sense: 5'-CTCCTTCAAGTTCGAGGACTT-3', antisense: 5'-AAGTCCTCGAACTTGAAGGAG-3').

GC cells plated in 6-well plates were exposed to viral particles in medium containing 5 μg/ml polybrene at a multiplicity of infection value of 20. Following incubation under standard conditions (37˚C, 5% CO_2), medium was replaced with a fresh complete medium and cultured the cells for another 48 h. The lentiviral transduction was conducted over 72 h. Successfully transduced cells were selected with 2.0 μg/ml puromycin for 48 h, followed by an additional 48 h recovery period in fresh complete medium prior to subsequent experiments.

Lactate content assay. Following the instructions of a commercial lactate content detection kit (Wuhan Servicebio Technology Co., Ltd.), for lactate assay, L-lactic acid was oxidized by a specific lactate oxidase to pyruvate and H_2O_2. In the presence of peroxidase and chromogens, a colored dye was produced, which was measured photometrically at 546 nm. The absorbance of the dye, measured photometrically, was directly proportional to the L-lactic acid concentration. The results were normalized according to the total protein content.

ATP content assay. Following the instructions of the ATP content detection kit (Wuhan Servicebio Technology Co., Ltd.), ATP assay was based on the principle that luciferase catalyzes the chemiluminescence reaction of luciferin under the energy provided by ATP, and within a certain range, the luminous intensity was directly proportional to the ATP content. The results were normalized based on the cell count.

Statistical analyses. Statistical analyses and data visualization were performed using GraphPad Prism software (v9.5.0; Dotmatics) and shown as the mean ± standard deviation (SD). Significance was determined using an unpaired two-tailed Student's t-test or one-way analysis of variance, followed by Tukey's multiple comparisons test. P<0.05 was considered to indicate a statistically significant difference.

Results

Oxaliplatin induces senescence in GC cells. To verify whether OXA induce senescence in GC cells, an *in vitro* model was established using AGS and MKN45 cells lines. Briefly, cells were assigned to control (Ctrl) and OXA groups. CCK-8 assays revealed that OXA reduced AGS and MKN45 cell viability in a concentration-dependent manner (Fig. S1A and B). Based on these results, AGS cells were treated with 2.5 μM OXA, while MKN45 cells were treated with 5 μM OXA, both for 48 h. Senescence was assessed through SA-β-Gal staining, western blotting, immunofluorescence detection of γ-H2AX, and qPCR analysis of SASP factors.

SA-β-Gal staining detects cellular senescence by measuring the SA-β-Gal activity at pH 6.0, which hydrolyzes X-Gal to generate a blue product (18). As presented in Fig. 1A, compared with the Ctrl group, OXA group displayed a greater percentage of SA-β-Gal-positive GC cells, along with enlarged and flattened morphology. Quantitative analysis confirmed

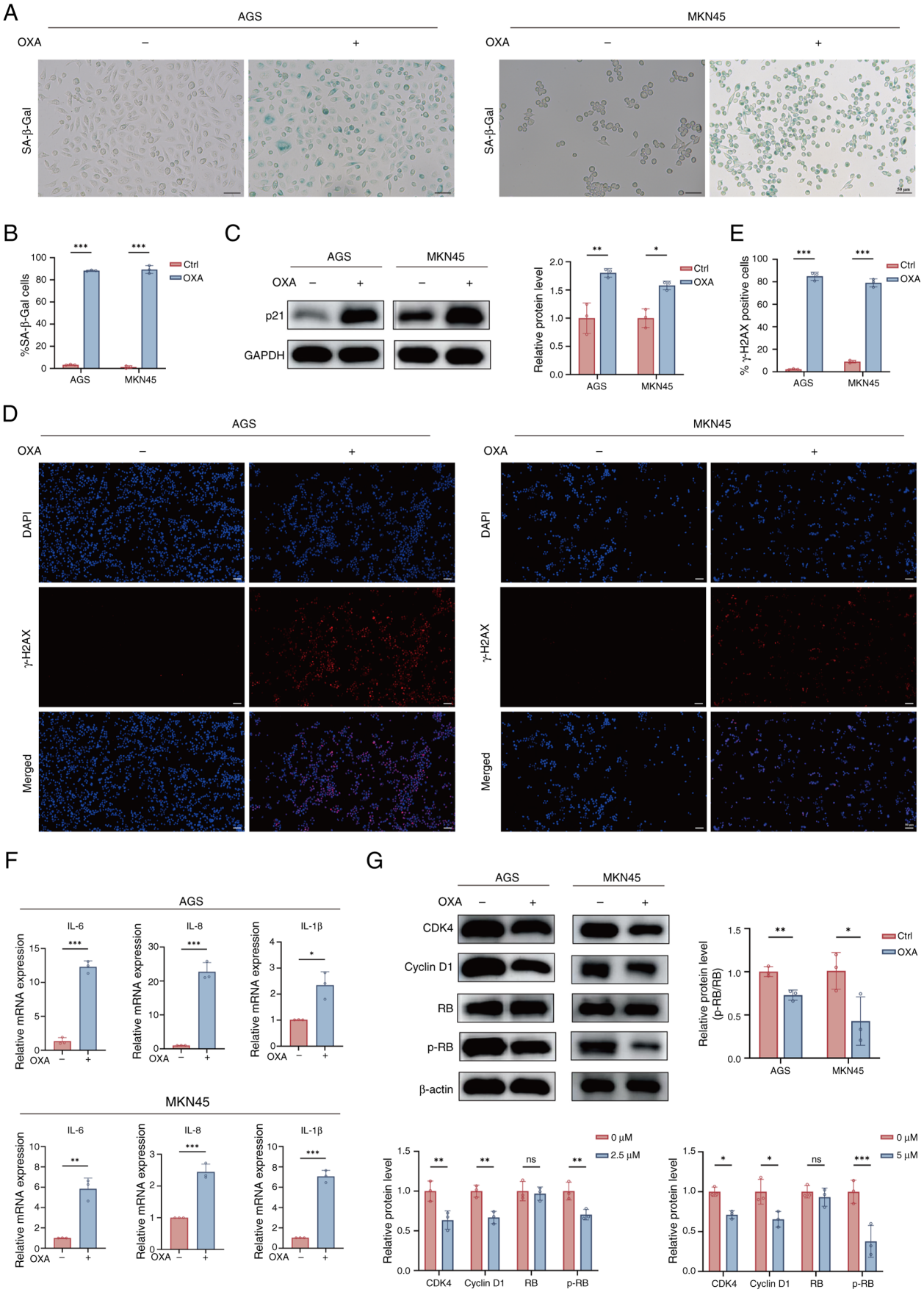

Figure 1. OXA induces senescence was verified in gastric cancer cells. (A and B) SA-β-Gal staining of Ctrl and OXA groups and quantification of SA-β-Gal positive cells in AGS and MKN45 cells. (C) p21 protein expression and quantification. (D and E) Immunofluorescence of γ-H2AX and quantification. Red fluorescence indicates γ-H2AX staining, and blue fluorescence reflects nuclear staining with DAPI. (F) mRNA levels of the senescence-associated secretory phenotype factors. (G) CDK4, cyclin D1, RB, p-RB protein expression, and quantification in the two groups. Data represent the mean ± SD of at least three independent experiments. *P<0.05, **P<0.01 and ***P<0.001. OXA, oxaliplatin; SA-β-Gal, senescence-associated β-galactosidase; p-, phosphorylated.

that the average SA-β-Gal positivity rates were 88.3% in AGS cells from the OXA group and 89.32% in MKN45 cells from the OXA group (Fig. 1B).

As a cyclin-dependent kinase inhibitor, p21 is a key mediator of cellular senescence (19). Western blotting indicated a significant upregulation of p21 protein in the OXA group compared with the Ctrl group, suggesting the induction of cell cycle arrest (Fig. 1C). Since γ-H2AX is a classic marker of DNA damage and replication stress and is a central driver of senescence induction (20), its expression was assessed. Immunofluorescence showed a stronger enhancement of γ-H2AX foci in OXA group than in Ctrl group (Fig. 1D and E).

SASP comprises the secretion of diverse inflammatory cytokines, chemokines and proteases, which affects the tumor microenvironment (TME) (21). Next, the mRNA expression levels of major SASP components were evaluated using RT-qPCR. RT-qPCR analysis indicated a significant upregulation of various SASP factors, such as interleukin (IL)-6, IL-8 and IL-1β in the OXA group relative to the Ctrl group in AGS and MKN45 cells (Fig. 1F).

Finally, to clarify the cell cycle regulatory network associated with senescence, the expression of key regulatory proteins was examined (22). Compared with the Ctrl group, CDK4 and cyclin D1 were significantly downregulated in OXA group; however, total RB protein levels remained unchanged, and p-RB levels decreased. These results suggested that after OXA induction, cell cycle progression was inhibited, and RB was maintained in a hypo-phosphorylated active state (Fig. 1G).

In summary, it was established that OXA induces senescence in AGS and MKN45 cells, as evidenced by elevated SA-β-gal activity, p21 upregulation, cell cycle regulator inhibition, DNA damage accumulation and enhanced SASP secretion.

Integrated transcriptomic and proteomic analyses identified the NR4A1-PI3K/AKT axis in chemotherapy-induced senescence. To systematically elucidate the molecular mechanisms of OXA-induced senescence in GC cells, integrative transcriptomic and proteomic analyses of AGS cells were performed by comparing Ctrl and OXA groups.

As demonstrated in Fig. 2A, the transcriptomic volcano plot revealed 1,536 DEGs in the OXA group ($|\log_2 FC| > 0.585$, $P < 0.05$) with 1,193 upregulated and 343 downregulated genes. Proteomic analysis further identified 2,047 proteins that were significantly altered ($|\log_2 FC| > 0.26$, $P < 0.05$), including 1,040 upregulated and 1,007 downregulated proteins. Venn diagram analysis exhibited that 224 molecules were consistently differentially expressed at both transcriptomic and proteomic levels (Fig. 2B), implicating a central role in OXA-induced senescence.

KEGG enrichment of the overlapping differentially expressed molecules revealed marked enrichment in pathways closely associated with senescence, tumor progression and metabolism, including 'p53 signaling pathway', 'PI3K-AKT signaling pathway', 'platinum drug resistance' and 'metabolic pathways' (Fig. 2C). Notably, the PI3K-AKT signaling pathway was significantly enriched at both omics' levels, highlighting its critical role in chemotherapy-induced senescence. The expression of PI3K-AKT pathway associated genes and their corresponding proteins, was then visualized using heatmaps (Fig. 2D).

Among these candidates, NR4A1 was explored, a stress-responsive nuclear receptor that is regarded as a key molecule linking signal transduction with metabolic fate. Emerging evidence indicates that NR4A1 regulates cellular metabolism and fate by suppressing PI3K/AKT signaling (23,24). It was discovered that in GC, NR4A1 expression was elevated at the transcriptional and protein levels in the OXA group. Consistent with this, qPCR (Fig. 2E) and western blotting (Fig. 2F) confirmed elevated NR4A1 expression in OXA group compared with the Ctrl group. Moreover, to enhance the clinical value of NR4A1, its prognostic significance was further analyzed using the TCGA-STAD dataset via GEPIA2. Notably, Kaplan-Meier survival analysis showed a shorter OS in patients with high relative to low NR4A1 expression (Fig. 2G).

Collectively, integrative multi-omics analyses indicate that OXA induces cellular senescence in GC cells by upregulating NR4A1 and suppressing the PI3K/AKT pathway. Notably, NR4A1 expression was induced during OXA-induced senescence *in vitro*, whereas intrinsically high NR4A1 expression was correlated with poor prognosis, indicating a context-dependent role of NR4A1 in GC.

NR4A1-PI3K/AKT axis promotes OXA-induced senescence in GC cells. To explore the role of NR4A1 in chemotherapy-induced senescence, NR4A1-knockdown AGS and MKN45 cell lines were generated using shRNA technology. Western blotting confirmed that NR4A1 protein levels were decreased in the sh-NR4A1 groups compared with the sh-NC group, with sh-NR4A1#2 exhibiting the most efficient knockdown (Fig. 3A). Consequently, sh-NR4A1#2 was selected for subsequent experiments.

The senescence marker p21 expression was first detected. As expected, p21 expression was significantly upregulated in the sh-NC + OXA group relative to the sh-NC group. However, this induction was significantly weakened in the sh-NR4A1#2 + OXA group (Fig. 3B). These results indicated that NR4A1 knockdown partially reversed the p21-mediated senescence signal triggered by OXA. Consistently, SA-β-Gal staining indicated that senescent cells increased substantially in the sh-NC + OXA group compared with sh-NC, while this increase was significantly reduced in the sh-NR4A1#2 + OXA group (Fig. 3C). Next, the SASP phenotype was assessed using RT-qPCR. High expression of typical SASP factors was found in the sh-NC + OXA group, but this upregulation was significantly reduced in the sh-NR4A1#2 + OXA group (Fig. 3D).

Based on the aforementioned findings, the PI3K-AKT pathway was highly enriched in transcriptomic and proteomic analyses, and it was further explored whether NR4A1 was involved in regulating this pathway. For this purpose, levels of phosphorylated AKT at Ser473 (p-AKT) and total AKT, core indicators of PI3K/AKT pathway activity, were analyzed by western blotting. It was found that the sh-NC + OXA group significantly suppressed AKT phosphorylation (decreased p-AKT/AKT ratio). This suppression was effectively reversed in the sh-NR4A1#2 + OXA group, in which the p-AKT/AKT ratio was restored (Fig. 3E).

In conclusion, NR4A1 is a critical regulator of OXA-induced senescence in GC cells. NR4A1 knockdown weakened p21 upregulation, SA-β-Gal positivity and SASP secretion,

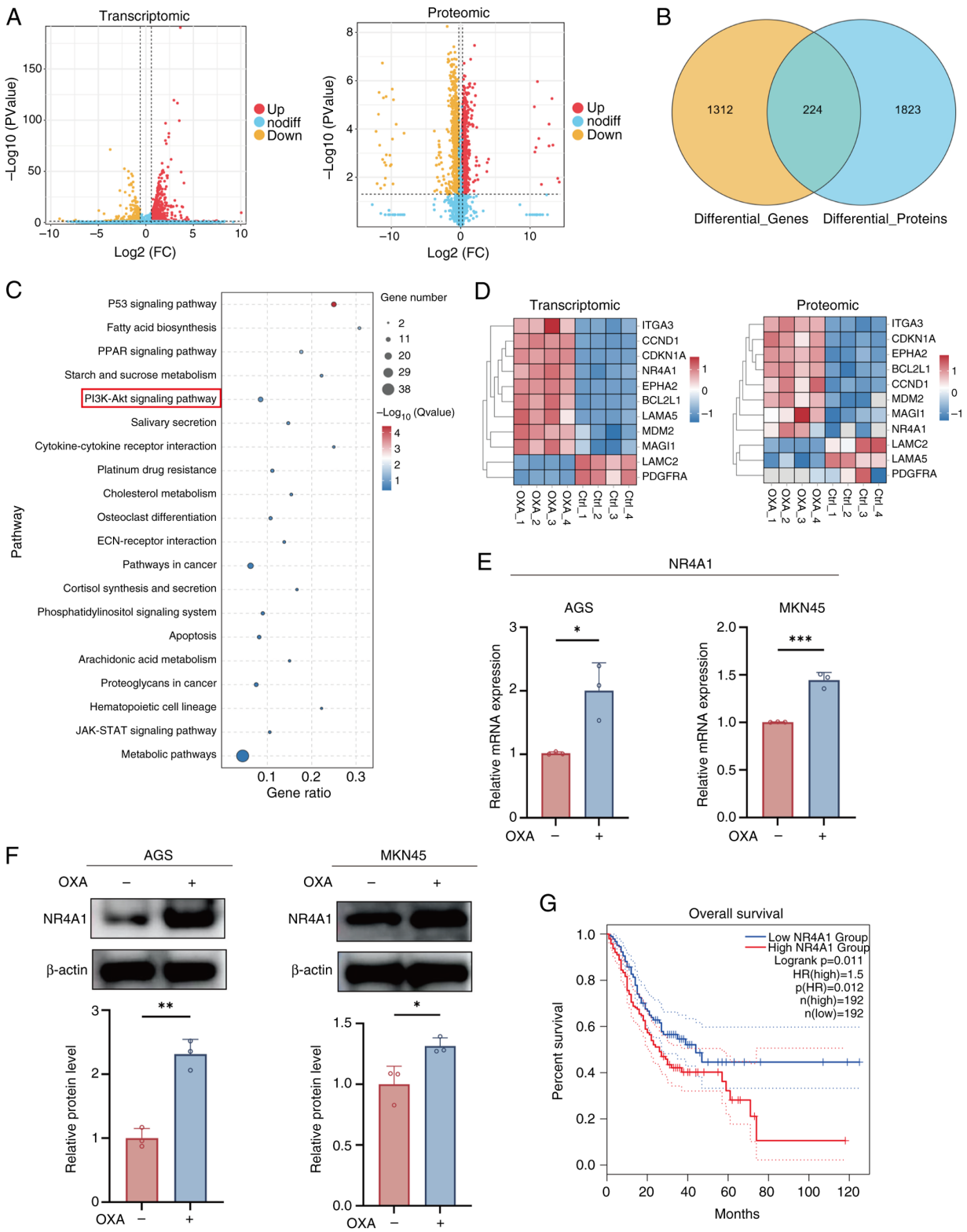

Figure 2. Integrated analyses of transcriptomic and proteomic data identify the NR4A1-PI3K/AKT axis in chemotherapy-induced senescence. (A and B) Volcano plot of RNA-sequencing data illustrating differentially expressed genes and proteins between Ctrl and OXA groups. (C) Kyoto Encyclopedia of Genes and Genomes enrichment analysis of the same differentially expressed molecules at both the omics levels. (D) Heatmaps exhibit transcriptomic and proteomic expression patterns of genes and proteins associated with the PI3K/AKT pathway. (E and F) NR4A1 expression is validated by reverse transcription-quantitative PCR and western blotting with quantitative analysis. (G) Kaplan-Meier survival analysis of NR4A1 in patients with gastric cancer based on GEPIA2. Data represent the mean ± SD of at least three independent experiments. *P<0.05, **P<0.01 and ***P<0.001. OXA, oxaliplatin; HR, hazard ratio.

and restored PI3K/AKT-associated pathway activity. Collectively, these results highlight a central role for the NR4A1-PI3K/AKT axis in chemotherapy-induced cellular senescence.

NR4A1-PI3K/AKT axis-driven metabolic reprogramming. To assess metabolic alterations during chemotherapy-induced senescence, untargeted metabolomic profiling of AGS

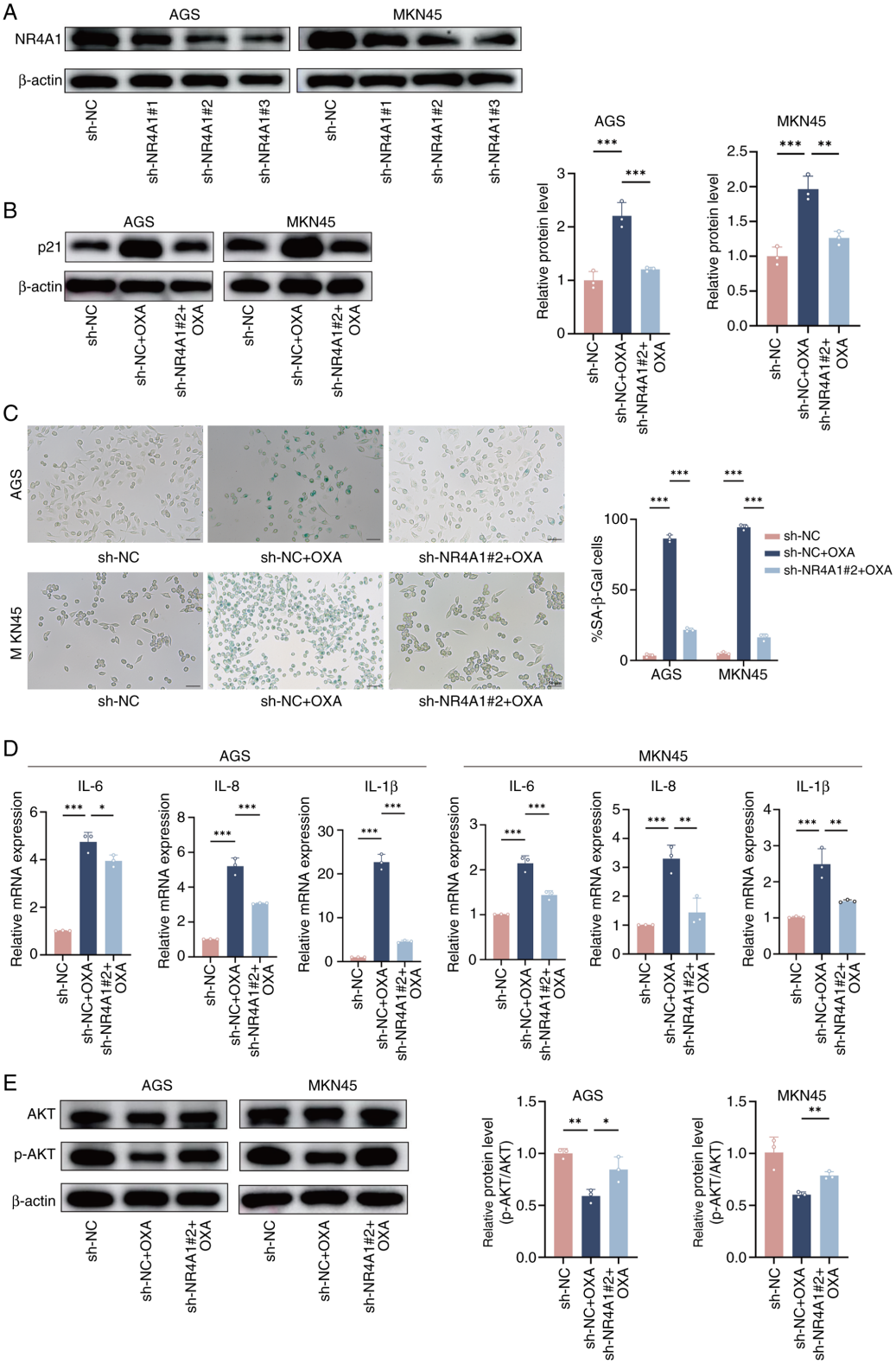

Figure 3. NR4A1 is identified as a key regulator of senescence, and the NR4A1-PI3K/AKT axis modulates OXA-induced senescence of gastric cancer cells. (A) Western blotting confirmed the efficiency of NR4A1 knockdown. (B and C) Western blotting and quantitative analysis of p21 expression and PI3K/AKT signaling activity (p-AKT/AKT ratio) in sh-NC, sh-NC + OXA, and sh-NR4A1#2 + OXA groups. (D) SA-β-gal staining and quantitative analysis of the positive cells. (E) Reverse transcription-quantitative PCR analysis of senescence-associated secretory phenotype factor expression across the experimental groups. Data represent the mean ± SD of at least three independent experiments. *P<0.05, **P<0.01 and ***P<0.001. OXA, oxaliplatin; sh-, short hairpin; NC, negative control; p-, phosphorylated.

cells was performed in Ctrl and OXA groups. Score plots demonstrated an obvious separation between Ctrl and OXA groups in neg and pos ion detection modes, indicating favorable reproducibility (Fig. 4A). Permutation tests further confirmed that the model fits well in both modes (Fig. 4B), supporting the metabolomic analysis stability. The

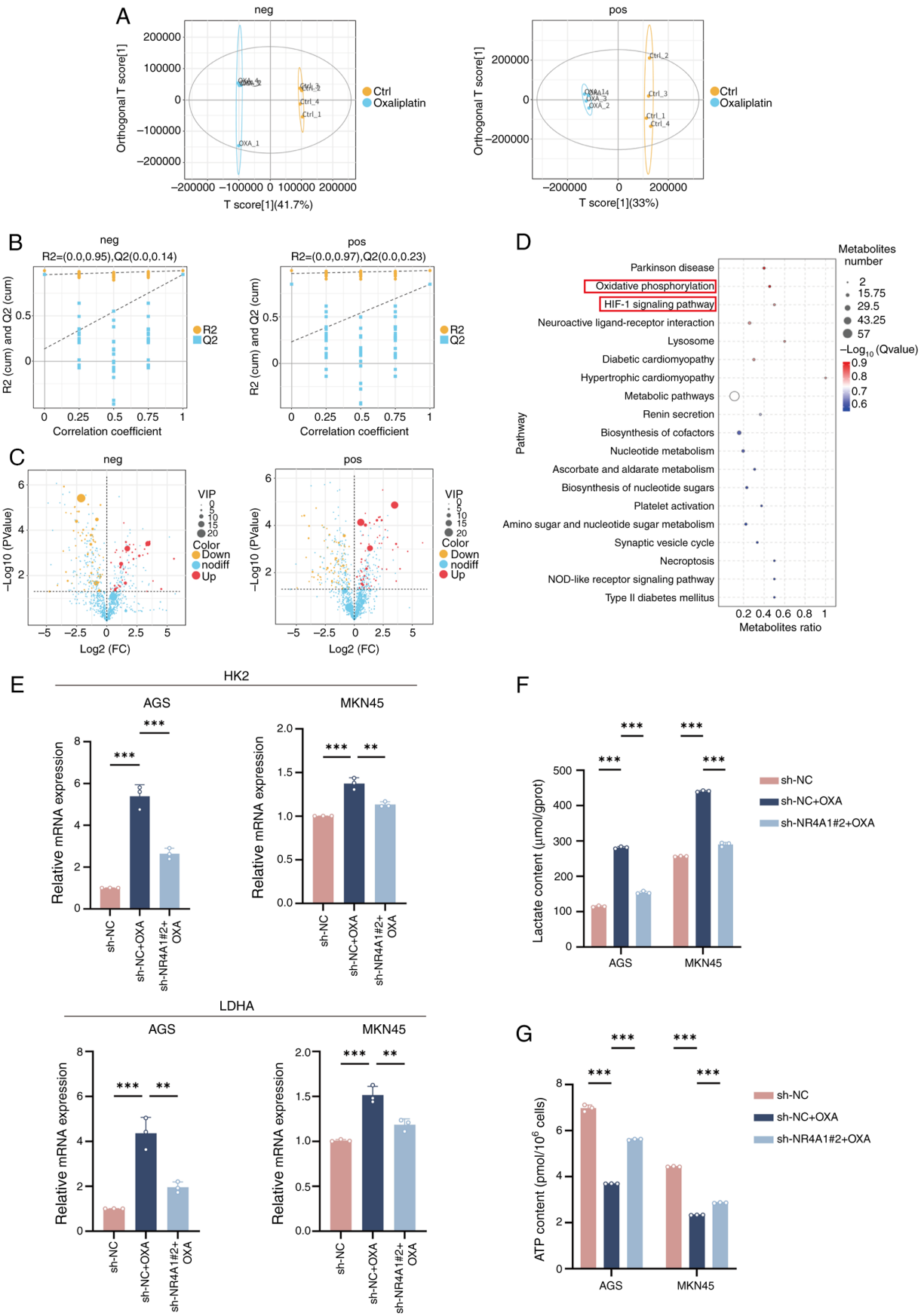

Figure 4. NR4A1-PI3K/AKT axis drives metabolic reprogramming in gastric cancer cells. (A) Score plots from multivariate statistical analysis of the neg and pos ion modes. (B) Permutation test plots validated the statistical model in neg and pos modes. (C) Volcano plots of differential metabolites in neg and pos modes. (D) Kyoto Encyclopedia of Genes and Genomes pathway enrichment analysis of metabolites in the combination of neg and pos modes. (E) Reverse transcription-quantitative PCR analysis of glycolytic genes LDHA and HK2, (F) lactate content assay and (G) ATP content assay in sh-NC, sh-NC + OXA and sh-NR4A1#2 + OXA groups. Data represent the mean ± SD of at least three independent experiments. **P<0.01 and ***P<0.001. LDHA, lactate dehydrogenase A; HK 2, hexokinase 2; OXA, oxaliplatin; sh-, short hairpin; NC, negative control.

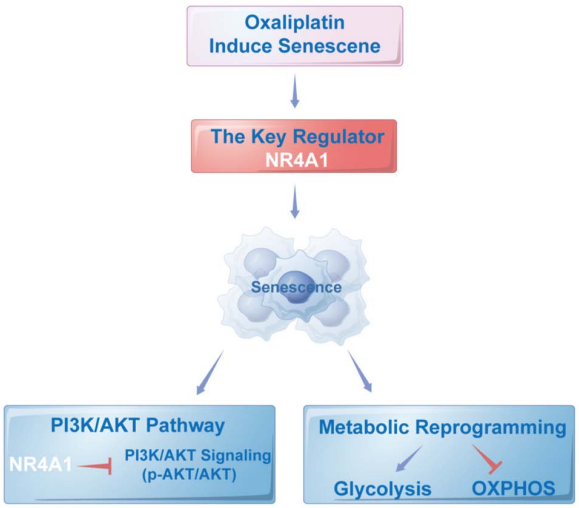

Figure 5. Schematic illustration of the NR4A1-PI3K/AKT-metabolic axis in chemotherapy-induced senescence of GC. This schematic diagram summarizes the molecular mechanism by which the NR4A1-PI3K/AKT-metabolic axis mediates chemotherapy-induced senescence in GC cells. GC, gastric cancer; OXPHOS, oxidative phosphorylation; p-, phosphorylated.

aforementioned results prove the stability of the experiment and the reliability of the observed metabolic differences. Differential metabolite analysis revealed pronounced metabolic alterations in the OXA group under both neg and pos ion modes. Specifically, 41 metabolites were upregulated and 66 downregulated in the neg mode, while 59 were upregulated and 76 downregulated in the pos mode (VIP >1, P<0.05) (Fig. 4C). Following integration of the differential metabolites from both neg and pos modes, KEGG pathway enrichment analysis was performed (Fig. 4D). The analysis indicated that these metabolites were substantially enriched in key metabolic pathways, including 'OXPHOS', 'HIF-1 signaling pathway', 'metabolic pathways' and 'nucleotide metabolism' (Fig. 4D). Notably, the significant enrichment of OXPHOS and HIF-1 signaling, two central energy metabolism pathways, was significantly enriched. This result suggests that OXA-induced senescence in GC cells may drive metabolic reprogramming by inhibiting OXPHOS and promoting glycolysis.

To verify the role of NR4A1 in metabolic reprogramming, the mRNA expression levels of key glycolytic enzymes were measured. RT-qPCR analysis demonstrated significant upregulation of lactate dehydrogenase A (LDHA) and hexokinase 2 (HK2) in the sh-NC + OXA group relative to the sh-NC group, whereas this effect was significantly reversed in the sh-NR4A1#2 + OXA group (Fig. 4E). The functional experiments supported these findings. Lactate levels were substantially increased in the sh-NC + OXA group and were significantly reduced in the sh-NR4A1#2 + OXA group (Fig. 4F). Concurrently, ATP detection showed a notable decrease in cellular ATP content in the sh-NC + OXA group relative to sh-NC, reflecting impaired OXPHOS function. Notably, ATP production was restored in the sh-NR4A1#2 + OXA group, exceeding that in the sh-NC + OXA group (Fig. 4G).

In conclusion, OXA-induced GC cells triggered extensive metabolic reprogramming characterized by OXPHOS inhibition and glycolysis enhancement ('Warburg effect'). NR4A1 is a central mediator of OXA-induced metabolic reprogramming. NR4A1 knockdown effectively reversed the upregulation of glycolytic genes (LDHA and HK2) by OXA, alleviated ATP generation suppression, and reduced lactate accumulation. Building on previous findings, these data demonstrate that NR4A1-mediated inhibition of the PI3K/AKT pathway serves as a novel bridge connecting chemotherapy-induced stress to metabolic reprogramming (Fig. 5).

Discussion

GC remains a major global health challenge and is a prominent cause of cancer deaths. Increasing evidence indicates that chemotherapy, particularly with platinum-based agents, can induce TIS. TIS has emerged as a unique cellular response with dual effects on tumors. While it limits tumor proliferation through stable cell cycle arrest, the accompanying SASP remodels the TME, which can promote immune evasion and contribute to recurrence. Accordingly, understanding the molecular mechanisms of chemotherapy-induced senescence in GC is essential for identifying actionable targets and optimizing therapeutic strategies. The present findings support previous studies that chemotherapy can induce TIS (25,26). It was first confirmed that OXA effectively induces a senescence phenotype in GC cells, characterized by p21 upregulation, elevated SA-β-Gal positivity, accumulation of γ-H2AX foci, and enhanced SASP secretion. Subsequently, through integrated transcriptomic and proteomic analyses, it was observed that the PI3K/AKT pathway is critical for senescence regulation and NR4A1 was further identified as a potential regulator of TIS. Functional experiments demonstrated that NR4A1 negatively regulates the PI3K/AKT pathway, consistent with previous studies (27,28).

In parallel, metabolomic profiling revealed that OXA-induced senescence was accompanied by typical metabolic reprogramming, namely, enhanced glycolysis and suppressed OXPHOS. These observations strongly support the emerging concept of 'metabolism-senescence combination' (29,30). Based on these findings, it was demonstrated that NR4A1 knockdown reversed OXA-induced metabolic reprogramming, which was reflected by the downregulation of glycolytic enzymes (LDHA and HK2), restored ATP production, and reduced lactate accumulation. Collectively, these results indicate that NR4A1 improves the establishment and stabilization of the senescent phenotype by maintaining PI3K/AKT signaling in a low-activity state and driving an imbalance between glycolysis and energy metabolism.

The present *in vitro* findings demonstrate that NR4A1 is upregulated under OXA-induced stress and promotes a stable senescent state by suppressing PI3K/AKT signaling and metabolic reprogramming. However, clinical cohorts reveal a paradoxical observation between high NR4A1 expression and poor prognosis in patients with GC. This discrepancy can be explained by the context-dependent nature of NR4A1 biology (31). *In vitro*, NR4A1 elevation represents a short-term stress response that drives tumor cells toward proliferation arrest and senescence. Conversely, persistently

elevated NR4A1 levels in tumors likely reflect a distinct long-term program involving metabolic adaptation, chronic inflammation, or an immunosuppressive microenvironment, all of which are features commonly associated with adverse outcomes (32).

Moreover, TIS can inhibit proliferation in the short term; however, persistent SASP can promote immune evasion, angiogenesis, EMT, and ultimately facilitate tumor recurrence or drug resistance. Therefore, NR4A1-driven senescence may simultaneously confer short-term growth inhibition and long-term tumor progression risk, consistent with the observed survival association (33). Notably, tumors with high NR4A1 expression, despite being more aggressive, may be more dependent on the NR4A1-mediated senescence pathway, and therefore, more sensitive to chemotherapy-induced senescence. In summary, the current mechanistic findings highlight the acute and pro-senescence effects of NR4A1, whereas clinical data reflect its complex and long-term association with tumor biology. Collectively, these findings reveal that NR4A1 has dual and temporally distinct roles in GC.

From a clinical standpoint, TIS represents a 'double-edged sword' in which it inhibits tumor progression and facilitates immune evasion and tumor recurrence due to SASP secretion. Therefore, the recently proposed 'one-two punch' strategy, which involves the induction of senescence followed by targeted senolysis, represents a promising anti-cancer therapeutic strategy (34-36). In the present study, findings suggest that the intervention of the NR4A1-PI3K/AKT axis and the NR4A1-metabolic axis may collectively amplify the tumor-suppressive effect of therapy-induced senescence. However, they simultaneously provide new opportunities for senolytic and SASP-modulating interventions. This strategy could potentially improve chemosensitivity and reduce drug resistance and recurrence risk.

The present study provides two major innovations. First, it was proposed that NR4A1 acts as an important regulator of chemotherapy-induced senescence in GC. Second, the relationship between the NR4A1-PI3K/AKT axis and metabolic reprogramming was revealed, providing a new idea for enhancing the aging effect through metabolic intervention and offering a theoretical basis for metabolic-targeted anti-cancer therapy. Nevertheless, the present study has certain limitations. Firstly, experiments were primarily reliant on GC cell models, which necessitates future validation in other types of cancer to determine whether the observed mechanisms are widely applicable. Second, future studies should analyze the NR4A1 regulatory network and explore its potential in combination with immunotherapy or metabolic therapy.

In conclusion, the present study established NR4A1 as an important mediator of OXA-induced senescence in GC cells. It acts by suppressing the PI3K/AKT pathway and driving metabolic transitions characterized by impaired OXPHOS and enhanced glycolysis. The present study provides innovative mechanistic insights into the interaction between chemotherapy, signaling pathways and metabolic plasticity, and highlights NR4A1 as a promising therapeutic target for enhancing senescence-based strategies. Interventions targeting the NR4A1-PI3K/AKT-metabolic axis may amplify the tumor-suppressive effect of therapy-induced senescence while reducing its tumorigenic consequences, offering a reasonable framework for the integration of 'one-two punch' strategies or immunotherapy.

Acknowledgements

Not applicable.

Funding

The present study was supported by the Precision Medicine Joint Cultivation Fund Project of Natural Science Foundation of Hebei (grant no. H2021402007), the Basic Research Special Project of Natural Science Foundation of Hebei (grant no. H2022402009), the Cooperative Project of the Affiliated Hospital of Hebei University of Engineering (grant no. KFKT2024-05), the Scientific Research Project of the Administration of Traditional Chinese Medicine of Hebei (grant no. 2022149) and the Handan Clinical Medicine Excellent Talent Project (grant no. ZF2023221).

Availability of data and materials

The data generated in the present study may be found in the Open Archive of the China National Center for Bioinformation under accessions numbers HRA015931, OMIX014177 or OMIX014178, or at the following URL: https://ngdc.cncb.ac.cn/.

Authors' contributions

TZ designed the research, conducted the experiments and wrote the manuscript. YW assisted with the experiments and data analysis. JZ and XY contributed to data analysis and participated in data discussion. YS contributed to data interpretation, participated in data discussion and critically revised the manuscript. ZZ contributed to study conception, experimental design, and critical revision of the manuscript. TZ and ZZ confirm the authenticity of all the raw data. All authors read and approved the final version of the manuscript.

Ethics approval and consent to participate

Not applicable.

Patient consent for publication

Not applicable.

Competing interests

The authors declare that they have no competing interests.

References

1. Bray F, Laversanne M, Sung H, Ferlay J, Siegel RL, Soerjomataram I and Jemal A: Global cancer statistics 2022: GLOBOCAN estimates of incidence and mortality worldwide for 36 cancers in 185 countries. CA Cancer J Clin 74: 229-263, 2024.

2. Mikula-Pietrasik J, Niklas A, Uruski P, Tykarski A and Ksiazek K: Mechanisms and significance of therapy-induced and spontaneous senescence of cancer cells. Cell Mol Life Sci 77: 213-229, 2020.
3. Faheem MM, Seligson ND, Ahmad SM, Rasool RU, Gandhi SG, Bhagat M and Goswami A: Convergence of therapy-induced senescence (TIS) and EMT in multistep carcinogenesis: Current opinions and emerging perspectives. Cell Death Discov 6: 51, 2020.
4. Takasugi M, Yoshida Y and Ohtani N: Cellular senescence and the tumour microenvironment. Mol Oncol 16: 3333-3351, 2022.
5. Wang L, Lankhorst L and Bernards R: Exploiting senescence for the treatment of cancer. Nat Rev Cancer 22: 340-355, 2022.
6. McHugh D, Duran I and Gil J: Senescence as a therapeutic target in cancer and age-related diseases. Nat Rev Drug Discov 24: 57-71, 2025.
7. Pan W, Tan Y, Chen X, Zeng L, Lv Y and Yang J: miRNA-204-5p acts as a tumor suppressor in gastric cancer by inhibiting cell migration, invasion, and glycolysis via the RAB22A/PI3K/AKT axis. Sci Rep 15: 29536, 2025.
8. Yan S, Hu X, Wu Y, Ye W, Zhu Y, He Y, Zhan F, Wu W and Ma Z: ITGA4 contributes to 5-fluorouracil resistance by Up-Regulating PI3K/AKT signaling: evidence from network pharmacology, molecular docking and experimental verification. Drug Des Devel Ther 19: 4105-4122, 2025.
9. Fontana F, Giannitti G, Marchesi S and Limonta P: The PI3K/Akt pathway and glucose metabolism: A dangerous liaison in cancer. Int J Biol Sci 20: 3113-3125, 2024.
10. Zhang CY, Tan XH, Yang HH, Jin L, Hong JR, Zhou Y and Huang XT: COX-2/sEH dual inhibitor alleviates hepatocyte senescence in NAFLD mice by restoring autophagy through Sirt1/PI3K/AKT/mTOR. Int J Mol Sci 23: 8267, 2022.
11. Tang Q, Markby GR, MacNair AJ, Tang K, Tkacz M, Parys M, Phadwal K, MacRae VE and Corcoran BM: TGF-β-induced PI3K/AKT/mTOR pathway controls myofibroblast differentiation and secretory phenotype of valvular interstitial cells through the modulation of cellular senescence in a naturally occurring in vitro canine model of myxomatous mitral valve disease. Cell Prolif 56: e13435, 2023.
12. Efimova EV, Appelbe OK, Ricco N, Lee SS, Liu Y, Wolfgeher DJ, Collins TN, Flor AC, Ramamurthy A, Warrington S, *et al*: O-GlcNAcylation enhances double-strand break repair, promotes cancer cell proliferation, and prevents therapy-induced senescence in irradiated tumors. Mol Cancer Res 17: 1338-1350, 2019.
13. Gu J, Wang J, Liu X, Sai K, Mai J, Xing F, Chen Z, Yang X, Lu W, Guo C, *et al*: IL-6 derived from therapy-induced senescence facilitates the glycolytic phenotype in glioblastoma cells. Am J Cancer Res 11: 458-478, 2021.
14. Mikula-Pietrasik J, Witucka A, Pakula M, Uruski P, Begier-Krasinska B, Niklas A, Tykarski A and Ksiazek K: Comprehensive review on how platinum- and taxane-based chemotherapy of ovarian cancer affects biology of normal cells. Cell Mol Life Sci 76: 681-697, 2019.
15. Melones-Herrero J, Alcala S, Ruiz-Canas L, Benitez-Buelga C, Batres-Ramos S, Cales C, Lorenzo O, Perona R, Quiroga AG, Sainz B Jr and Sanchez-Perez I: Platinum iodido drugs show potential anti-tumor activity, affecting cancer cell metabolism and inducing ROS and senescence in gastrointestinal cancer cells. Commun Biol 7: 353, 2024.
16. Livak KJ and Schmittgen TD: Analysis of relative gene expression data using real-time quantitative PCR and the 2(-Delta Delta C(T)) Method. Methods 25: 402-408. 2001.
17. Tang Z, Kang B, Li C, Chen T and Zhang Z: GEPIA2: an enhanced web server for large-scale expression profiling and interactive analysis. Nucleic Acids Res 47 (W1):W556-W560, 2019.
18. Lee BY, Han JA, Im JS, Morrone A, Johung K, Goodwin EC, Kleijer WJ, DiMaio D and Hwang ES: Senescence-associated beta-galactosidase is lysosomal beta-galactosidase. Aging Cell 5: 187-195, 2006.
19. Yan J, Chen S, Yi Z, Zhao R, Zhu J, Ding S and Wu J: The role of p21 in cellular senescence and aging-related diseases. Mol Cells 47: 100113, 2024.
20. Biran A, Zada L, Abou Karam P, Vadai E, Roitman L, Ovadya Y, Porat Z and Krizhanovsky V: Quantitative identification of senescent cells in aging and disease. Aging Cell 16: 661-671, 2017.
21. Dong Z, Luo Y, Yuan Z, Tian Y, Jin T and Xu F: Cellular senescence and SASP in tumor progression and therapeutic opportunities. Mol Cancer 23: 181, 2024.
22. Gorgoulis V, Adams PD, Alimonti A, Bennett DC, Bischof O, Bishop C, Campisi J, Collado M, Evangelou K, Ferbeyre G, *et al*: Cellular senescence: Defining a path forward. Cell 179: 813-827, 2019.
23. Ma YL, Kong CY, Guo Z, Wang MY, Wang P, Liu FY, Yang D, Yang Z and Tang QZ: Semaglutide ameliorates cardiac remodeling in male mice by optimizing energy substrate utilization through the Creb5/NR4a1 axis. Nat Commun 15: 4757, 2024.
24. Li JM, Song ZH, Li Y, Chen HW, Li H, Yuan L, Li J, Lv WY, Liu L and Wang N: NR4A1 silencing alleviates high-glucose-stimulated HK-2 cells pyroptosis and fibrosis via hindering NLRP3 activation and PI3K/AKT pathway. World J Diabetes 16: 97544, 2025.
25. Kallenbach J, Atri Roozbahani G, Heidari Horestani M and Baniahmad A: Distinct mechanisms mediating therapy-induced cellular senescence in prostate cancer. Cell Biosci 12: 200, 2022.
26. Zhang D, Zhang JW, Xu H, Chen X, Gao Y, Jiang HG, Wang Y, Wu H, Yang L, Wang WB, *et al*: Therapy-induced senescent tumor cell-derived extracellular vesicles promote colorectal cancer progression through SERPINE1-mediated NF-κB p65 nuclear translocation. Mol Cancer 23: 70, 2024.
27. Wang H, Wei Z, Xu C, Fang F, Wang Z, Zhong Y and Wang X: Nuclear receptor 4A1 ameliorates UUO-induced renal fibrosis by inhibiting the PI3K/AKT pathway. Sci Rep 14: 24787, 2024.
28. Lei L, Guo Q, Cheng Y, Gui Y, Li W, Zhao Y, Xu Z, Luo Y, Wu G, Wang JZ, *et al*: Age-dependent elevation of Nr4a1 attenuates PI3K/AKT/GSK3beta pathway and mediates tau hyperphosphorylation and cognitive impairments. J Adv Res S2090-1232(25)00442-4, 2025 (Epub ahead of print).
29. Kirkland JL and Tchkonia T: Cellular senescence: A translational perspective. EBioMedicine 21: 21-28, 2017.
30. Herranz N and Gil J: Mechanisms and functions of cellular senescence. J Clin Invest 128: 1238-1246, 2018.
31. Safe S and Karki K: The paradoxical roles of orphan nuclear receptor 4A (NR4A) in cancer. Mol Cancer Res 19: 180-191, 2021.
32. Ma QX, Yin M and Lei QY: A nucleotide regulates NR4A1 status in gastric cancer. Mol Cell 85: 4299-4300, 2025.
33. Faget DV, Ren Q and Stewart SA: Unmasking senescence: Context-dependent effects of SASP in cancer. Nat Rev Cancer 19: 439-453, 2019.
34. Wang C, Vegna S, Jin H, Benedict B, Lieftink C, Ramirez C, de Oliveira RL, Morris B, Gadiot J, Wang W, *et al*: Inducing and exploiting vulnerabilities for the treatment of liver cancer. Nature 574: 268-272, 2019.
35. Qing Y, Li H, Zhao Y, Hu P, Wang X, Yu X, Zhu M, Wang H, Wang Z, Guo Q and Hui H: One-Two punch therapy for the treatment of T-Cell malignancies involving p53-dependent cellular senescence. Oxid Med Cell Longev 2021: 5529518, 2021.
36. Wang T, Liu W, Shen Q, Tao R, Li C, Shen Q, Lin Y, Huang Y, Yang L, Xie G, *et al*: Combination of PARP inhibitor and CDK4/6 inhibitor modulates cGAS/STING-dependent therapy-induced senescence and provides 'one-two punch' opportunity with anti-PD-L1 therapy in colorectal cancer. Cancer Sci 114: 4184-4201, 2023.